SAND2015-10698C

Measurements of Gas-Phase Velocity During Shock-Particle Interactions Using Pulse-Burst PIV

Edward P. DeMauro[*] Justin L. Wagner[†] Steven J. Beresh[‡] and Paul A. Farias[§]

Sandia National Laboratories, Albuquerque, NM 87111, USA

High-speed, time-resolved particle image velocimetry with a pulse-burst laser was used to measure the gas-phase velocity upstream and downstream of a shock wave-particle curtain interaction at three shock Mach numbers (1.19, 1.40, and 1.45), at a sampling rate of 37.5 kHz. Using this data, and data collected from unsteady pressure taps upstream/downstream of the curtain, a control volume analysis was performed in order to determine the curtain drag as a function of time. The particle curtain, formed from free-falling soda-lime particles with diameters ranging from 300 - 355 μm, had a streamwise thickness of 3.5 mm and volume fraction of 9% at mid-height. Following impingement of the initial shock wave on the curtain, spreading of the particle curtain in the streamwise direction was observed, under the influence of drag. Initially dominated by the pressure difference upstream/downstream of the curtain, the drag first begins to decrease due to equilibration of the pressures, followed by a gradual increase associated with acceleration of the downstream flow field.

Nomenclature

a	Speed of sound (m/s)
A_c	Cross-sectional area (m^2)
g	Acceleration due to gravity (= 9.81 m/s^2)
H	Test section's height (m)
$\dot{m}_{mix}$	Mass flow rate of air/particle mixture (kg/s)
M_s	Shockwave Mach number
t	Time (s)
t_0	Reference time when shock reaches curtain (s)
t^*	$\frac{U_{ind}}{h}(t - t_0)$
t_δ	$\frac{\delta}{U_{ind}}$ (s)
u	Unsteady streamwise velocity (m/s)
u_p	Particle velocity (m/s)
v	Unsteady wall-normal velocity (m/s)
U_{ind}	Velocity induced by passage of shock wave (m/s)
V_{tot}	Total velocity (m/s)
x	Streamwise direction (m)
y	Wall-normal direction (m)
z	Spanwise direction (m)
δ	Particle curtain's streamwise thickness (m)
φ_p	Particle curtain's volume fraction

---

[*] Postdoctoral Appointee, Engineering Sciences Center, P.O. Box 5800, MS-0825, Albuquerque, NM 87125, Member AIAA. Corresponding author: epdemau@sandia.gov

[†] Senior Member of the Technical Staff, Engineering Sciences Center, P.O. Box 5800, MS-0825, Albuquerque, NM 87125, Member AIAA.

[‡] Distinguished Member of the Technical Staff, Engineering Sciences Center, P.O. Box 5800, MS-0825, Albuquerque, NM 87125, Associate Fellow AIAA.

[§] Senior Technologist

ρ_{air}	Density of air (kg/m^3)
ρ_{mix}	Density of particle/gas mixture (kg/m^3)
ρ_p	Density of particles (kg/m^3)
$\forall_{mix}$	Volume of particle/gas mixture (m^3)
$\forall_p$	Volume of particles (m^3)

I. Introduction

An understanding of the complex physics associated with the interaction of a shock wave with a multiphase mixture is important in many engineering applications. These include such areas as pulsed detonation engines,[1, 2] mining safety,[3] rocket propulsion,[4] and dispersion of heterogeneous mixtures.[5] When a shock wave interacts with a multiphase mixture, momentum and energy are exchanged. In addition, most of these interactions involve clouds or agglomerations of solid or liquid particles. The difficulty therefore arises in that the inter-particle interactions (collisions) and the aerodynamics of the particles in the presence of a highly compressible flow (i.e. drag) combine to make sound predictions difficult.[6]

A solid-gas mixture may be divided into one of three categories based on volume fraction (φ_p): dilute (φ_p $< 1\%$), granular ($50\% < \varphi_p$), and an intermediate, dense gas-solid regime ranging from $1\% \leq \varphi_p \leq 50\%$.[5] In this sense, dilute mixtures form an extreme where the volume of the solid particles are negligible in relation to the volume of the gas, such as a fine dust. In comparison, granular mixtures contain solid particle volumes that are greater than or equal to the volume of fluid within the mixture. In these mixtures, interactions between the particles cannot be neglected, as the particles may in fact be in direct contact with each other.[5] Finally, dense mixtures are those mixtures where the solid volume is non-negligible, but the particles are not themselves closely packed. Studies of the interaction of a shock wave with a sold-gas mixture therefore may be grouped together according to the mixture regime under investigation.

Within the literature, a variety of studies have been performed to measure the interaction of a shock wave with a dilute solid-gas mixture. Outa et al.[7] used pressure measurements to study the decay a shock wave propagating through a dilute cloud of particles. Marconi et al.[8] performed a numerical investigation of a shock wave propagating through a dusty cloud of varying thicknesses, noting the sensitivity of the propagated shock wave to a number of parameters such as particle size and concentration. Rudinger[9] noted difficulty in standard drag models' prediction of the dispersal of particles within a dusty cloud. Sommerfeld[10] attempted to define a new drag law for particles within this regime, developing a power law valid for only a limited range of Mach numbers, and dependent on Reynolds number. Boiko et al.[11] experimented with larger volume fractions ($0.1\% \leq \varphi_p \leq 3\%$) and noted the formation of a reflected shock wave propagating back upstream of the associated particle clouds, an observation also noted by Geng & Groenig.[12]

There has been much discussion recently regarding the true nature of particle drag following impingement of a shock wave on a dilute solid-gas mixture. Although it has been known that the standard drag model fails in its underestimation of particle drag following this interaction, more recent work has shown that this discrepancy is not due to unsteadiness in the long term.[13, 14] Parmer et al.[14] showed that unsteady loading was largely limited to the transient associated with a shock wave passing over a given particle, quickly dissipating to negligible values thereafter. Furthermore, their study concluded that drag measurements tended to rapidly asymptote towards quasi-steady predictions. Using a custom-built Multiphase Shock Tube (*MST*) designed for conducting experiments on solid-gas flows, Wagner et al.[15] demonstrated that unsteadiness did not appear to contribute to long-time drag behavior in dilute solid-gas mixtures, rather that the particle drag showed a strong Mach number dependence, in agreement with Parmer et al.[14] In addition, work by Martinez et al.[16] has looked to refine measurements of particle drag within a dilute flow by directly measuring particle acceleration and positions as functions of time.

Using the *MST* facility, Wagner et al. performed experiments on the interaction of a particle curtain with a dense solid-gas mixture.[17, 18] These tests were performed on a particle curtain formed of soda-lime particles with a diameter of 100 μm, resulting in a streamwise volume fraction of 20%. From high-speed Schlieren and unsteady pressure measurements, the formation of a reflected and transmitted shock wave emanating from the curtain post-interaction with the shock wave (similar to what was seen by Boiko et al.[11]) was observed, along with spreading of the particle curtain in the streamwise direction.[17] Work by Ling et al.[6] developed a new drag law model that incorporated unsteadiness, compressibility, volume fraction, and inter-particle interaction effects, which was seen to be able to better model the behavior of the particle curtain after the shock wave interaction, in comparison to using a standard drag model. Contrary to dilute mixtures, it was seen that, in the case of dense mixtures, unsteadiness had a prolonged contribution to the curtain drag over prolonged time. In addition to these, further work on the dense mixture regime include Regele et al.[19] who performed a two-dimensional simulation to improve on the one-dimensional results of Ling et al.,[6] Liu et al.[20] who suggested dependencies on particle initial temperature and restitution coefficient in are important in an interaction model, and Kellenberger[21] who performed dense mixture tests in a shock tube using a densely packed *particle wafer*.

The work presented here is a continuation of the work shown in Wagner et al.[17] The study performed here makes use of a pulse-burst laser, which is capable of producing high-repetition rates (up to 500 kHz) of ∼50 mJ/pulse. Using this laser, time-resolved particle image velocimetry (*TR-PIV*) measurements are presented on the gas-phase velocity upstream and downstream of the particle curtain, during interaction with a planar shock wave. The results of these measurements, along with unsteady pressures, are then used to in order to perform a control volume analysis in order to calculate the total drag imposed on the particle curtain as a function of time.

II. Experimental Setup

The multiphase shock tube (*MST*) is shown in Fig. 1. The driver section of the shock tube was constructed from a 2.1 m long stainless steel pipe with an inner diameter of 89 mm and a wall thickness of 12.7 mm, supplied with a high pressure nitrogen source. The driven section consists of square tubing, 5.2 m long, with an inner width of 76 mm and wall thickness of 12.7 mm. The driven gas was air at an initial temperature and absolute pressure of 300 K and 84.1 kPa, respectively. In lieu of burst discs, a Dynamics Systems Research (Model 183-1.5-2000) fast acting valve was used to fire the shock tube. The fast valve was used in these experiments due to its repeatability and comparably rapid turn-around time.

Experiments were conducted at three shock Mach numbers: M_s = 1.19, 1.40, and 1.45, which corresponded to driver pressures of 690, 2070, and 2760 kPa. Prior to an experiment, soda lime particles rested on an initially closed gate valve. When the gate valve was opened, particles (under the influence of gravity) flowed through a beveled slit through the test section ceiling, measuring $\delta = 3.5$ mm in streamwise thickness. The experiments presented here were performed using particles with a diameter distribution of 300 - 355 μm. These larger particles were utilized in comparison to the previous work of Wagner et al.;[17] the reason for this will be elaborated on shortly. The particles exited the test section through a similar slit in the floor, where they entered a particle collector reservoir. Prior to the start of a test, the particle curtain was allowed to flow through the test section for 1 s in order to ensure that steady state has been reached within the curtain. The slit, with a spanwise width of 68.6 mm (87% of the test section width), shaped the particles into the desired particle curtain. From this slit, the particle curtain was measured to flow at a rate (within 95% confidence) of 52.6 ± 0.25 g/s.

Prior to conducting all experiments, an extensive set of tests were conducted in order to characterize and quantify the particle curtain. These included measurements of the particle velocity, mass flow rate, and curtain thickness. As the particles free-fall from the open slit, their velocity increases under the influence of gravity; i.e. $u_p(y) \approx \sqrt{2g(y+H/2)}$. Assuming a constant cross-sectional area, A_c, the density of the particle curtain, as a function of height, can be shown to be:

$$\rho_{mix}(y) = \frac{\dot{m}_{mix}}{u_p(y)A_c} \tag{1}$$

where u_p is the velocity of the particles. Since the volume fraction can vary across the height of the particle curtain, the volume fraction (φ_p) reported in this study corresponded to that measured at mid-height, determined from:

$$\varphi_p = \frac{\forall_p}{\forall_{mix}} = \frac{\rho_{mix} - \rho_{air}}{\rho_p - \rho_{air}} \tag{2}$$

The resulting curtain further narrowed to a streamwise thickness of about 2 mm for the bottom 75% of the test section height. Figure 2 shows the particle curtain, acquired at an oblique angle, along with a back-lit image of the curtain used to measure the curtain thickness. Under the assumption of a uniform particle distribution, the particle volume fraction was measured to be ∼9% at the center of the curtain (∼91% void fraction) corresponding to a converging curtain.[22] Note that in reality, the particle distribution within the curtain is Gaussian,[18,19,23] however, for purposes of simplicity, this was assumed to be a negligible factor.

At this height, the particles were measured to flow at a velocity of 0.89 m/s, which corresponds free fall;[23] therefore they were essentially frozen in comparison to the shock velocities.

Previous *PIV* measurements in shock tubes have typically been difficult due to low repetition rates, allowing for few realization to be obtained in the millisecond test times of a shock tube and/or low energy per pulse.[24–27] Recent advances and the commercialization of pulse-burst laser technology, however, have made time-resolved *PIV* (*TR-PIV*) in high-speed flows a feasible and attractive option to overcome this limitation.[28] For this study, the light source for the *TR-PIV* was a Quasi-Modo (Spectral Energies, LLC) burst-mode laser, with a repetition rate of 37.5 kHz, which provided ∼25 mJ per pulse. The duration of the burst was 10.5 ms, greater than the typical test times in the *MST*. The laser was operated in a doublet (i.e. double pulsed) mode, where the time delay between pulses was set to $\delta t = 4\ \mu$s. As was previously mentioned, the larger sized particles were used in this experiment in order to decrease the number of particles entering into the *TR-PIV* camera fields of view, where scattering from the soda-lime particles would overpower the intensity of scattered light from seed particles.

Typical sheet-forming optics were used to shape the laser into two separate 1.5 mm thick laser sheet, as seen in Fig. 3. Two Photron SA-Z cameras, each with a resolution of 680 pixels × 340 pixels, were placed side-by-side to extend the field-of-view while maintaining spatial resolution. Each camera was operated at 75 kHz in order to frame-straddle the 37.5 kHz doublets. Seed particles were produced using a TSI six-jet atomizer, introduced into the shock tube about 0.5 m downstream of the fast acting valve. In-situ measurements showed that the atomizer gave a particle size of ∼1.6 μm; this resulted in Stokes numbers ranging from 0.025 - 0.061, depending on flow conditions. Raw images were processed with the LaVision DaVis 8.2 software package using a multi-pass method, with an initial interrogation window size of 64 × 64 pixels with 50% overlap, followed by two iterations performed with an interrogation window size of 32 × 32 pixels at a 75% overlap. Spurious vectors associated soda-lime particle light scattering were removed using a vector range filter; remaining errors were addressed with a median filter with a 5 × 5 universal outlier detector.

Due to excessive reflections from the particle curtain and limitations associated with the camera bodies, both upstream and downstream fields of view were offset 19 mm from the centerline of the particle curtain, as shown in Fig. 3. Therefore, Schlieren imaging was also performed in order to visualize the direct interaction of the shock wave with the particle curtain, along with the resulting relevant flow features. The light source for the Schlieren was a Visual Instrumentation Corporation continuous-wave high brightness LED (Model 900415). Two 101.6 mm planoconvex lenses with a focal length of ∼1 m were used; the first to collimate the light before entry into the test section. The secondary planoconvex lens focused to light exiting the test section onto a vertical knife-edge. Images were acquired using a Photron SA-Z camera, with a resolution of 680 pixels × 340 pixels, operating at a framing rate of 75 kHz.

Finally, pressure measurements were conducted using four PCB pressure sensors (Model 113B27), which collected time-resolved measurements at a rate of 800 kHz (two upstream and two downstream of the curtain) placed at $x/H =$ -1.04, -0.72, 0.40, and 0.72, along the centerline. In addition, both the *TR-PIV* and Schlieren measurements were triggered off of a single PCB sensor (Model 113B26) located 0.5 m downstream of the fast acting valve.

III. Results/Discussion

The results/discussion will be broken into two primary subsections. In the first subsection, the flow within the empty test section is presented; the second subsection discusses measurements collected with the goal of performing a control volume analysis, resolving the unsteady drag on the particle curtain. Note that the results are reported within a laboratory frame of reference. In order to create uniformity in the definition of non-dimensional time, unless otherwise specified, the characteristic length scale to be used will be the test section height, h, which is a common length scale between the baseline and particle curtain cases.

A. Baseline Flow

The baseline flow of the shock tube is shown in Fig. 4 for the $M_s = 1.40$ shock wave, at four separate times, represented by color contours of total velocity with in-plane velocity vectors. In addition, Schlieren imaging (collected in a subsequent test) is used to visualize the region that exists between the two *TR-PIV* fields of view. Initially, the gas within the driven section of the shock tube is quiescent, as seen in Fig. 4a. The initial shock can be seen here to be relatively planar. As time increases to t^* = -0.10 (Fig. 4b), the shock wave enters the Schlieren image, at $x/H \approx$ -0.25. As the shock wave moves downstream of the Schlieren image, into the downstream *TR-PIV* field of view, a series of weaker upstream-propagating, curved waves can be seen within the Schlieren (Fig. 4c and d). These shock waves are associated with reflections off of the edges of the particle curtain entrance and exit orifices, centered around $x/H = 0$.

Across this time, there is a measurable acceleration within the core flow, as can be from Fig. 5.[29] This acceleration is associated with boundary layer growth along the surfaces of the shock tube. This acceleration results in only small changes to the core velocity across the time of the test. These results show good agreement with those of Wagner et al.,[30] demonstrating repeatability. Note that there is a discrepancy associated with $M_s = 1.19$; this is possibly due to the formation of a secondary shock wave, leading to an additional increase in the induced velocity. This would be caused by non-ideal effects associated with actuation of the fast acting valve at the lower driver pressures required to obtain this test condition.

B. Interaction With The Particle Curtain

1. *Schlieren imaging of curtain interaction*

Schlieren imaging is presented in Fig. 6, highlighting particular features of the shock wave-particle curtain interaction. These representative images correspond to the $M_s = 1.40$ shock wave. The normal shock wave approaches the upstream side of the particle curtain at t^* = -0.10 (Fig. 6a); due to the large disparity between the shock wave speed and the speed of the particles within the curtain (0.89 m/s), the particles appear to be frozen. In Fig. 6b, the shock wave has now reached the particle curtain, resulting in the formation of a transmitted shock wave downstream of the curtain and a reflected shock wave that travels back upstream.

The reflected shock wave moves slower than the transmitted shock wave, as is clear from Fig. 6c and d. A summary of the shock Mach numbers can be seen in Table 1. In addition to this difference in speed, both shock waves are slightly inclined due to the wall-normal variation in volume fraction of the curtain.

Table 1. : Shock Wave Mach Numbers

Initial	Transmitted	Reflected
1.19	1.23	0.77
1.40	1.36	0.61
1.45	1.42	0.55

Referring to Eq. (1) to Eq. (2), it can be seen that, as $u_p \to 0$, $\varphi_p \to \infty$; i.e. the particle curtain becomes more porous closer to the bottom of the test section. Therefore, the reflected shock wave contains more energy where the volume fraction is largest (at the top of the test section), and less energy where the volume fraction is smallest (at the bottom), resulting in the inclined shock wave evident in Fig. 6d. Although not as readily apparent, the transmitted shock wave also is slightly inclined. It is expected that the change in curtain volume fraction as a function of height should induce two-dimensionalities within the gas phase upstream and downstream of the curtain, which will be explored in more detail in the following section.

The particle curtain itself does not immediately respond to the presence of the shock wave. The initial shock wave travels with a speed of U_s = 486 m/s; using the induced velocity of U_{ind} = 198.4 m/s, it is anticipated that the particle time of flight of the curtain (at mid-height) should be on the order of t_δ = 17.64 μs, based on the streamwise thickness of the particle curtain at mid-height. Deformation of the particle curtain begins in Fig. 6d, under the action of the total curtain drag at t^* = 0.30, resulting in a time lag of $\sim$108 μs, which is equal to $\sim 6t_\delta$. This value of $6t_\delta$ is common across all three interaction conditions tested, representing the non-dimensional time lag between impingement of the initial shock wave on the particle curtain and beginning of the curtain deformation process.

Deformation of the particle curtain is caused by a mismatch in the gas-phase velocities upstream and downstream of the curtain. As will be shown subsequently, the upstream traveling reflected shock wave decelerates the flow upstream of the particle curtain to a magnitude slower than that downstream of the curtain. This can be seen qualitatively, beginning in Fig. 6e, where the downstream side of the curtain begins moving downstream itself. By Fig. 6f, the upstream edge of the curtain has also begun to move in the streamwise direction, albeit at a slower rate.

Recall that the true streamwise volume fraction of the curtain (prior to impingement of the initial shock wave) contains a Gaussian distribution in the streamwise direction, with the maximum volume fraction centered at $x/H = 0$. As was seen by Wagner et al.,[18] as time increases, this absolute maximum is shifted downstream, resulting in a skewed distribution. Along with the streamwise widening of the particle curtain, the curtain volume fraction begins to decrease in time, creating a decreasing resistance to gas-phase flow. At $t^* = 1.24$ (Fig. 6g), this decreasing volume fraction is not readily apparent; however, beginning with $t^* = 1.90$ (Fig. 6h), light begins to penetrate through the upstream side of the curtain, implying a localized increase in porosity. The process continues at $t^* = 2.57$ and 3.24 (Fig. 6i and j), where further breakdown of the particle curtain results in increasing porosity becoming more evident within the upstream portion of the curtain. Note that the images in Fig. 6 encompass a total length of time lasting ∼1.3 ms.

2. Time-resolved PIV measurement of upstream/downstream flows

Although the Schlieren images of the shock wave/particle curtain interaction can shed much light qualitatively on the dynamics of the curtain, it leaves many questions unanswered. In contrast, *TR-PIV* of the gas phase upstream and downstream of the particle curtain can provide further insight into (1) the unsteady drag on the curtain and (2) whether the height-distribution of the curtain volume fraction could result in two-dimensionalities within the gas phase.

Color contours of total velocity with in-plane velocity vectors at five separate times are shown in Fig. 7 - Fig. 9, for $M_s = 1.19$, 1.40, and 1.45, respectively. Many features of the interaction appear to be repeatable among the three different Mach numbers. Initially a planar shock wave is visible at times leading up to impingement with the curtain (Fig. 7a, 8a, 9a). As shown in Fig. 6, the interaction with the particle curtain results in the formation of a transmitted and a reflected shock wave, both slightly inclined away from the curtain (Fig. 7b-c, 8b-c, 9b-c).

As the transmitted shock wave enters into the downstream field of view, the induced flow that it generates initially appears rather steady (compared to later times) for the $M_s = 1.40$ and 1.45 cases, seen in Fig. 8d and Fig. 9d, respectively, whereas there seems to be a larger degree of unsteadiness apparent at $M_s = 1.19$ (Fig. 7d). This may, once again, be a bi-product of the double initial shock wave associated with non-ideal actuation of the fast valve at this lower driver pressure. With increasing time, the degree of unsteadiness grows in all three cases, an observation that will be elaborated on later.

The inclined reflected and transmitted shock waves imply that a small wall-normal velocity component should be generated within the gas-phase flows. Figure 10a, c, and e shows color contours of V_{tot} with in-plane streamlines, corresponding to $t^* = 0.36$, 0.70, and 0.89, respectively. In addition, to better highlight the increased two-dimensionalities, the corresponding contours of wall-normal velocity, V, are also shown in Fig. 10b, d, and f. The reflected shock wave induces a wall-normal velocity directed towards the floor of test section, upstream of the curtain (Fig. 10b, d, and f). Similarly, a stronger positive wall-normal velocity is consistently formed downstream of the particle curtain (Fig. 10b, d, and f). Comparing the wall-normal velocity contours (Fig. 10b, d, and f) with the V_{tot} contours (Fig. 10a, c, and e), it is apparent that the upstream negative wall-normal velocity is a consequence of the inclined reflected shock. The downstream positive wall-normal velocity appears to also be a consequence of the slight inclination in the transmitted shock (best evident in Fig. 7c, Fig. 8c, and Fig. 9c, towards the top of the field of view). In addition to the wall-normal velocity, an acceleration of the downstream induced flow is consistently seen (Fig. 7e-g, Fig. 8e-g, Fig. 9e-g). When the shock wave impinges on the particle curtain, the reflected shock, propagating back upstream, increases the pressure upstream of the particle curtain, while reducing the upstream gas-phase velocity. Downstream of the curtain, the pressure is lower in comparison to the upstream pressure (implied by larger velocities), resulting in a favorable pressure gradient that accelerates flow through the curtain. Because both shock waves are tilted (upstream more than the downstream), the portion of the shock wave pointed back towards the particle curtain contains less energy than the rest of the shock wave, resulting in a $\partial u/\partial y$ (and therefore a $\partial v/\partial x$) velocity gradient.

Unsteadiness downstream of the particle curtain increases as a function of time, as shown in Fig. 7d, e, Fig. 8d, e, and Fig. 9d, e. One question that arises is whether or not this is a measure of small scale unsteadiness induced by flow past individual particles within the curtain. Initially, the length scales associated with particle-induced turbulence are on the order of 0.3 mm. In contrast, the vector resolution of the data in Fig. 7 - Fig. 9 is ∼0.8 mm; therefore, these vector fields lack the spacial resolution necessary to properly resolve turbulent length scales less than or equal to the vector resolution. However, as the curtain begins to deform in the manner described in Fig. 6, the streamwise volume fraction of the particle curtain decreases, increasing the interstitial spacing between particles; likewise, jetting becomes increasingly evident downstream of the curtain. As time increases, the length scales associated with this jetting grow; in addition, with increasing distance downstream of the curtain, these jets entrain flow from their surroundings and each other. Therefore, the jetting seen in Fig. 7g, Fig. 8g, and Fig. 9g represent larger scale motions than particle-induced turbulence.

3. *Time traces of unsteady measurements*

The unsteady streamwise velocity (averaged across the height of the measurement domain) and the time-resolved pressure data upstream and downstream of the curtain at $x/H = \pm\ 0.72$, are shown in Fig. 11. Prior to performing calculations of the curtain drag, 6^{th} degree polynomials were fit to the unsteady data, with their associated R^2 values given in Fig. 11. For the velocity data, this simplified performing operations such as taking time-derivatives. It should be noted that the pressure curve fits were performed using a much longer length of time, effectively smoothing out fluctuations. Early in the upstream pressure trace, a series of (relatively) low frequency oscillations can be seen at $t < 2$ ms. For now, these oscillations have not been incorporated into the analysis, given that the presence of these oscillations does not appear to be recognizable within the velocity data.

Given that the upstream data represents measurements prior to $t^* = 0$, the initial shock wave can be seen in Fig. 11a in the upstream time trace as a sudden jump at $t \approx$ -0.2 ms. The transmitted shock reaches the downstream sensor faster than the reflected shock reaches the upstream sensor, as can be seen in both Fig. 11a and b. The *TR-PIV* measurements encompass a timespan of $t < 1$ ms; it is clear from Fig. 11 that, within this time, the pressure upstream of the curtain is in fact larger than the pressure downstream. As time increases, however, it can be seen that the downstream pressure achieves a value greater than the upstream ($t > 2$ ms), and then begins to steadily decrease. This is due to the spreading of the particle curtain, moving downstream past the sensor location, resulting in false inaccurate measurements. The steady decrease in pressure towards the upstream pressure value therefore is mostly due to the bulk of the curtain propagating past the sensor.

4. *Estimation of particle curtain sectional drag*

To reiterate, the overarching goal of this study was to resolve the unsteady drag imposed on the particle curtain as a function of time. For this reason, a control volume approach was used to estimate the total drag. The streamwise momentum equation is:

$$\Sigma F_x = (P_1 - P_2)H - D' = \frac{\partial}{\partial t}\iint \rho u dx dy + \int \rho u^2 dy \tag{3}$$

where P_1 and P_2 are the upstream and downstream pressures, respectively; D' is the drag on the curtain per unity depth; ρ is the density of the gas phase, and u is the gas-phase velocity.

Integrating Eq.(3) results in:

$$D' = (P_1 - P_2)H + \delta x\left[\left(\frac{\rho_1 u_1^2}{\delta x} + \frac{\partial \rho_1 u_1}{\partial t}\right)H - \int_{-\frac{h}{2}}^{\frac{h}{2}}\left(\frac{\rho_2 u_2^2}{\delta x} + \frac{\partial \rho_2 u_2}{\partial t}\right)dy\right] \tag{4}$$

where δx is the streamwise length of the measurement domain. Equation (4) can be simplified further if u_2 is assumed constant across the height of the test section (i.e. an average value). In order to solve Eq. (4), it is necessary to have measurements of the pressure upstream and downstream of the curtain, along with the corresponding densities (two thermodynamic state variables). Further simplification results in:

$$D' = \rho_1 u_1^2 H\left[1 + \frac{P_1 - P_2}{\rho_1 u_1^2} - \frac{\rho_2}{\rho_1}\left(\frac{u_2}{u_1}\right)^2 + \frac{\delta x}{\rho_1 u_1^2}\frac{\partial}{\partial t}\left(\rho_1 u_1 - \rho_2 u_2\right)\right] \tag{5}$$

Since the previous measurements have shown that the induced flow fields upstream and downstream of the particle curtain are in fact two-dimensional, Eq. (4) provides only an estimate of the unsteady drag.

The terms in Eq. (5) represent the change in momentum and pressure across the particle curtain. The pressure difference across the boundaries of the control volume is given by:

$$\left(P_1 - P_2\right)H = \Delta P H$$

Likewise, the difference in momentum flux across the same boundaries is:

$$\left(\rho_1 u_1^2 - \rho_2 u_2^2\right) H = \Delta \rho u^2 H$$

Finally, the change in the rate change of momentum with time:

$$\delta x H \frac{\partial}{\partial t}\left(\rho_1 u_1 - \rho_2 u_2\right) = \frac{\partial \Delta\left(\rho u\right)}{\partial t} \delta x H$$

Prior to implementation of Eq. (5), a curve fit was applied to the experimental data for times ranging from after passage of the reflected shock wave in the upstream field of view until the particle curtain entered the downstream field of view. This was done in order to facilitate determination of the time derivatives in Eq. (5). With regards to the pressure measurements, a curve fit was also implemented in order to provide for interpolated values at time steps that corresponded with *TR-PIV* measurements. Values of density were from 1D compressible flow equations and were assumed constant after the passage of each respective shock wave.

The resulting drag on the curtain and the percentage contribution of each term are shown in Fig. 12a and b, respectively, for $M_s = 1.40$. The drag appears to be large at $t^* = 0$, decreasing with time until around a value of $t^* \approx 1.4$. From Fig. 8f and e, it is clear that this time corresponds to the beginning of the large jetting that appears downstream of the particle curtain. In comparison with the other components, the pressure difference across the boundaries of the control volume provides the largest single contribution to the total value of drag within the depicted time span (Fig. 12b), exhibiting a similar trend to the total drag as a function of time. However, as can be seen from the slopes, given enough time, the pressure contribution should approach zero as the upstream and downstream conditions equilibrate. The change in momentum flux, for example, increases from negative quantities towards zero, and slightly positive. Given the apparently larger, positive slope of the momentum flux term, it seems that as $t \to \infty$, this term could potentially dominate the total drag.

The increase in the momentum flux term is associated with acceleration of the core velocity (due to increased blockage associated with growing test section boundary layers). As was seen in Fig. 7, Fig. 8, and Fig. 9, the upstream gas-phase velocity becomes less than the downstream velocity once the reflected shock wave propagates through the field of view. However, the core velocity accelerates as a function of time (Fig. 5). This acceleration is apparent by the positive slope in the momentum flux difference, which begins to add to the overall drag in the curtain. Note that although the downstream velocity accelerates to values greater than the upstream, the upstream value of density (1.97 kg/m^3) is larger than the downstream density (1.59 kg/m^3). Finally, the rate change in momentum as a function of time was found to be relatively constant within the timescale of this calculation, with its percentage contribution to the overall drag appearing to almost asymptote.

IV. Conclusions

Experiments were conducted using *TR-PIV* with a pulse-burst laser and high-speed Schlieren imaging in order to make time-resolved measurements of the gas-phase velocity upstream and downstream of a particle curtain interaction with a shock wave. The purpose of these measurements was to collect the data necessary for determining the unsteady drag experienced by the particle curtain immediately following the shock wave interaction. The particle curtain was formed from soda-lime particles free-falling through a 3.2 mm slit, with a diameter ranging from 300 - 355 μm, resulting in a curtain with a streamwise volume fraction of 9% at mid-height. Three separate tests of the shock wave-particle curtain interaction were measured, at shock Mach numbers corresponding to $M_s = 1.19$, 1.40, and 1.45. In addition, time-resolved pressure measurements made upstream and downstream of the particle curtain allowed for the determination of the total drag on the curtain as a function of time.

When the initial shock wave impinged on the particle curtain, an upstream-propagating reflected shock wave, and a downstream-propagating transmitted shock wave were created. Following this impingement, a time-lag corresponding to $\sim 6 t_\delta$ was observed before the particle curtain began to deform due to the imposed drag. The variation of the particle curtain streamwise volume fraction as a function of height caused for the reflected shock wave to be inclined away from the particle curtain, whereas the transmitted shock wave was slightly inclined back towards the curtain, leading to the formation of two-dimensionalities within the respective induced gas-phase velocity fields.

The pressure difference between the upstream and downstream sides of the curtain encouraged flow to accelerate through the curtain, resulting in an increase in downstream gas-phase velocity. Furthermore, as time increased, the pressure difference across the curtain decreased. By calculating the drag on the curtain using a control volume method, it was shown that this pressure difference across the curtain initially contributes the largest percentage of drag to the total drag out of all the terms shown in Eq. (5). With increasing time, the pressure difference decreases, whereas the contribution associated with momentum flux across the boundaries of the control volume increases at a greater rate. These trends suggest that as time increases, the change in momentum flux may dominant over the pressure difference.

References

[1] Chang, E.J., and Kailasanath, K., "Shock wave interactions with particles and liquid fuel droplets," *Shock Waves*, Vol. 12, 2003, pp. 333-341.
doi: 10.1007/s00193-002-0170-1.

[2] Veyssiere, B., "Detonations in gas-particle mixtures," *Journal of Propulsion and Power*, Vol. 22, No. 6, 2006, pp. 1269-1288.
doi: 10.2514/1.18378.

[3] Merzkirch, W., and Bracht, K., "The erosion of dust by a shock wave in air: initial stages with laminar flow," *International Journal of Multiphase Flow*, Vol. 4, No. 1, 1978, pp/ 89-95.
doi: 10.1016/0301-9322(78)90028-9.

[4] Davis, S.L., Dittmann, T.B., Jacobs, G.B., and Don, W.S., "Dispersion of a cloud of particles by a moving shock: effects of the shape, angle of rotation, and aspect ratio," *Journal of Applied Mechanics and Technical Physics*, Vol. 54, No. 4, 2013, pp. 900-912.
doi: 10.1134/S0021894413060059.

[5] Zhang, F., Frost, D. L., Thibault, P. A., and Murray S. B., "Explosive dispersal of solid particles," *Shock Waves*, Vol. 10, 2001, pp. 431-443.

[6] Ling, Y., Wagner, J.L., Beresh, S.J., Kearney, S.P., and Balachandar, S., "Interaction of a planar shock wave with a dense particle curtain: modeling and experiments," *Physics of Fluids*, Vol. 24, 2012, pp. 1-30.
doi: 10.1063/1.4768815.

[7] Outa, E., Tajima, K., and Morii, H., "Experiments and analyses on shock waves propagating through a gas-particle mixture," *Bulletin of the JSME*, Vol. 19, No. 130, 1976, pp. 384-394.

[8] Marconi, F., Rudman, S., and Calia, V., "Numerical study of one-dimensional unsteady particle-laden flows with shocks," *AIAA Journal*, Vol. 19, No. 10, 1980, pp. 1294-1301.
doi: 10.2514/3.60063.

[9] Rudinger, G., "Some properties of shock relaxation in gas flows carrying small particles," *Physics of Fluids*, Vol. 7, No. 5, 1964, pp. 658-663.
doi: 10.1063/1.1711265.

[10] Sommerfeld, M., "The unsteadiness of shock waves propagating through gas-particle mixtures," *Experiments in Fluids*, Vol. 3, 1985, pp. 197-206.

[11] Boiko, V.M., Kiselev, V.P., Kiselev, S.P., Papyrin, A.N., Poplavsky, S.V., and Fomin, V.M., "Shock wave interaction with a cloud of particles," *Shock Waves*, Vol. 7, 1997, pp. 275-285.

[12] Geng, J.H., and Groenig, H., "Dust suspensions accelerated by shock waves," *Experiments in Fluids*, Vol. 28, No. 4, 2000, pp. 360-367.

[13] Sun, M., Saito, T., Takayama, K., and Tanno, H., "Unsteady drag on a sphere by shock wave loading," *Shock Waves*, Vol. 14, No. 1, 2004, pp. 3-9.
doi: 10.1007/s00193-004-0235-4.

[14] Parmer, M., Haselbacher, A., and Balachandar, S., "Modeling of the unsteady force for shock-particle interaction," *Shock Waves*, Vol. 19, 2009, pp. 317-329.
doi: 10.1007/s00193-009-0206-x.

[15] Wagner, J.L., Beresh, S.J., Kearney, S.P., Pruett, B.O.M., and Wright, E.K., "Shock tube investigation of quasi-steeady drag in shock-particle interactions," *Physics of Fluids*, Vol. 24, 2012, pp. 1-16.
doi:10.1063/1.4768816.

[16] Martinez, A.A., Orlicz, G.C., and Prestridge, K.P., "A new experiment to measure shocked particle drag using mult-pulse particle image velocimetry and particle tracking," *Experiments in Fluids*, Vol. 56, 2015, pp. 1-12.
doi: 10.1007/s00348-014-1854-x.

[17] Wagner, J. L., Beresh, S. J., Kearney, S. P., Trott, W. M., Castaneda, J. N., Pruett, B. O., and Baer, M. R., "A multiphase shock tube for shock wave interactions with dense particle fields," *Experiments in Fluids*, Vol. 52, 2012, pp. 1507-1517.
doi: 10.1007/s00348-012-1272-x.

[18] Wagner J.L., Kearney, S.P., Beresh, S.J., DeMauro, E.P., Pruett, B.O., "Flash X-Ray measurements on the shock-induced dispersal of a dense particle curtain," *Experiments in Fluids*, Vol. 56, No. 213, 2015, pp. 1-12.
doi: 10.1007/s00348-015-2087-3

[19] Regele, J.D., Rabinovitch, J., Colonius, T., and Blanquart, G., "Unsteady effects in dense, high speed, particle laden flows," *International Journal of Multiphase Flow*, Vol. 61, 2014, pp. 1-13.
doi: 10.1016/j.ijmultiphaseflow.2013.12.007.

[20] Liu, H., Guo, Y., and Lin, W., "Simulation of shock-powder interaction using kinetic theory of granular flow," *Powder Technology*, Vol. 273, 2015, pp. 133-144.
doi: 10.1016/j.powtec.2014.12.031.

[21] Kellenberger, M.D., *Dense particle cloud dispersion by a shock wave*, M.S. Thesis, Department of Mechanical and Materials Engineering, Queen's University, Kingston, On, 2012.

[22] Wardjiman, C., Lee, A., Sheehan, M., and Rhodes, M., "Shape of a particle curtain falling in stagnant air," *Powder Technology*, Vol. 192, 2009, pp.384-388.
doi: 10.1016/j.powtec.2009.01.009.

[23] Goetsch, R.J., and Regele, J.D., "Discrete element method prediction of particle curtain properties," *Chemical Engineering Science*, Vol. 137, 2015, pp. 852-861.
doi: 10.1016/j.ces.2015.07.034.

[24] Arakeri, J.H., Das, D., Krothapalli, A., and Lourenco, L., "Vortex ring formation at the open end of a shock tube: A particle image velocimetry study," *Physics of Fluids*, Vol. 16, No. 4, 2004, pp. 1008-1019.
doi: 10.1063/1.1649339.

[25] Prestridge, K., Rightley, P.M., Vorobieff, P., Benjamin, R.F., and Kurnit, N.A., "Simultaneous density-field visualization and PIV of a shock-accelerated gas curtain," *Experiments in Fluids*, Vol. 29, No. 4, 2000, pp. 339-346.

[26] Prestridge, K., Vorobieff, P., Rightley, P.M., and Benjamin, R.F., "Validation of an instability growth model using particle image velcimetry measurements," *Physical Review Letters*, Vol. 84, No. 19, 2000, pp. 4353-4356.

[27] Haehn, N., Weber C., Oakley, J., Anderson, M., Ranjan, D., and Bonazza, R., "Experimental investigation of a twice-shocked spherical gas inhomogeneity with particle image velocimetry," *Shock Waves*, Vol. 21, No. 3, 2011, pp. 225-231.
doi: 10.1007/s00193-011-0299-x.

[28] Beresh, S.J., Kearney, S.P., Wagner, J.L., Guildenbecher, D.R., Henfling, J.F., Spillers, R.W., Pruett, B.O.M., Jiang, N., Slipchenko, M.N., Mance, J., and Roy, S., "Pulse-burst PIV in a high-speed wind tunnel," AIAA Paper 2015-1218, Jan. 2015.
doi: 10.2514/6.2015-1218

[29] Mirels, H., "Flow nonuniformity in shock tubes operating at maximum test times," *Physics of Fluids*, Vol. 9, No. 10, 1966, pp. 1907-1912.

[30] Wagner J., Beresh, S., DeMauro, E., Casper K., Pruett, B., Farias, P., "Time-resolved PIV in a shock tube using a pulse-burst laser," 11th International Symposium on Particle Image Velocimetry - PIV15, Sept. 2015.

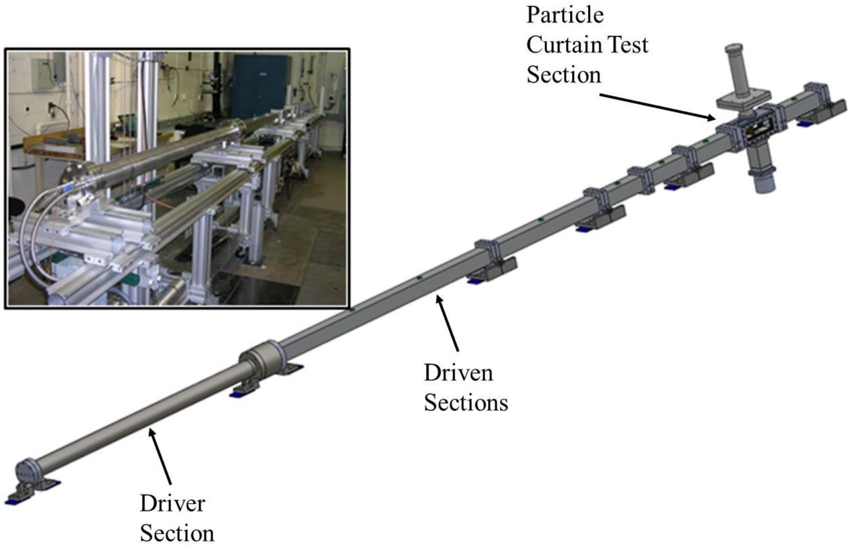

Figure 1. The multiphase shock tube (*MST*) with relevant sections identified.

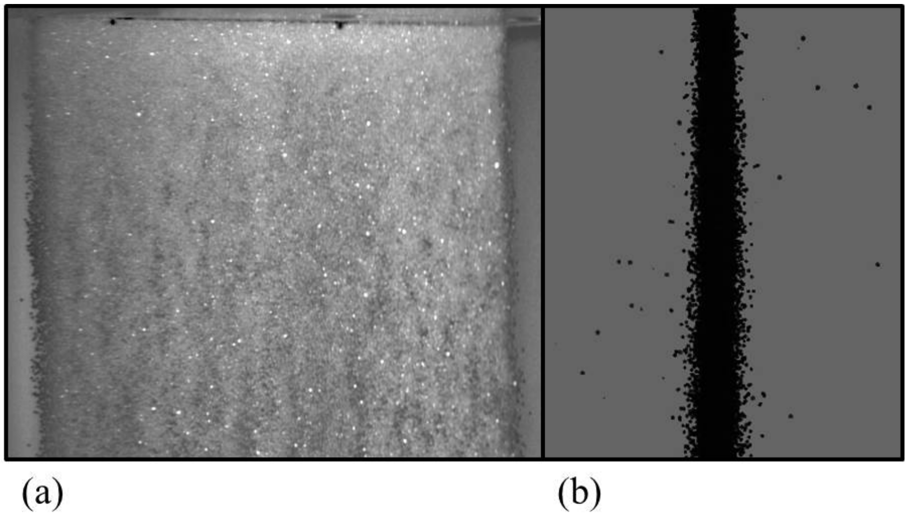

Figure 2. Instantaneous image of the particle curtain obtained at an oblique angle (a); instantaneous side-view of the particle curtain used to measure the curtain thickness (b). Note that a background subtraction has been performed in both images in order to highlight the relevant features.

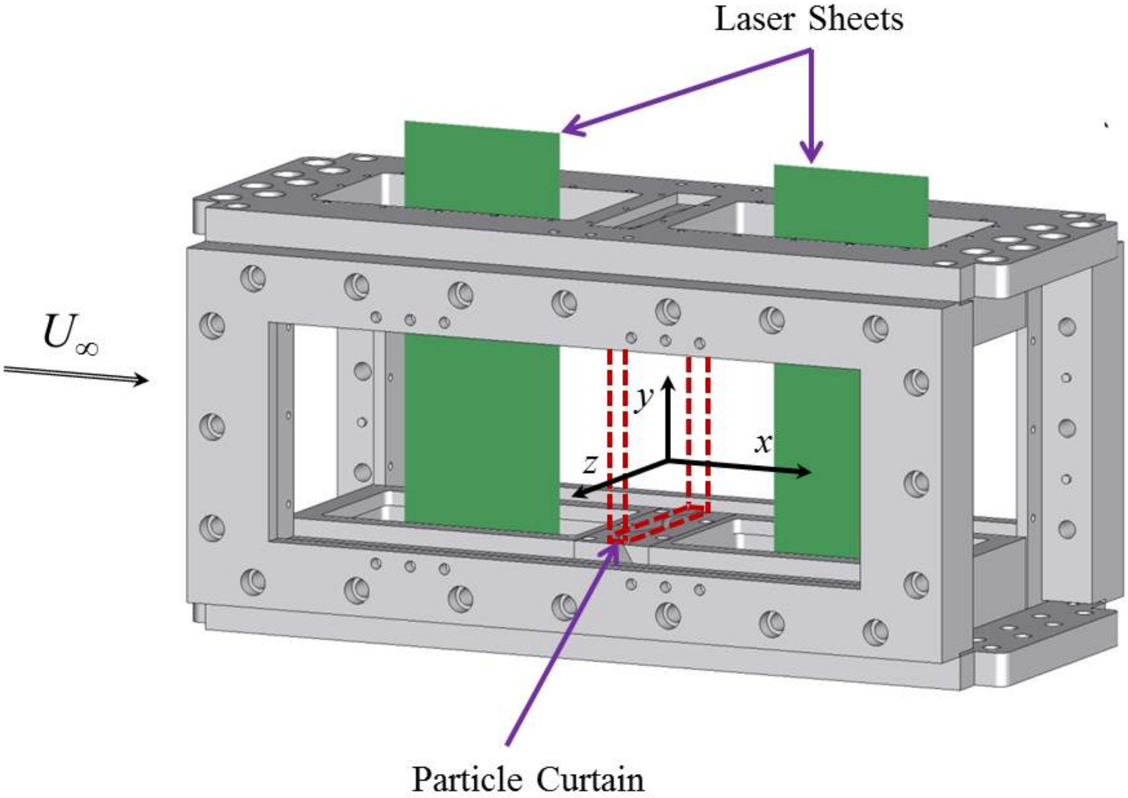

Figure 3. Schematic of the experimental setup with axis orientation, including upstream and downstream locations of *TR-PIV* measurements. The coordinate system is defined such that the origin is at mid-height in the center of the curtain slit.

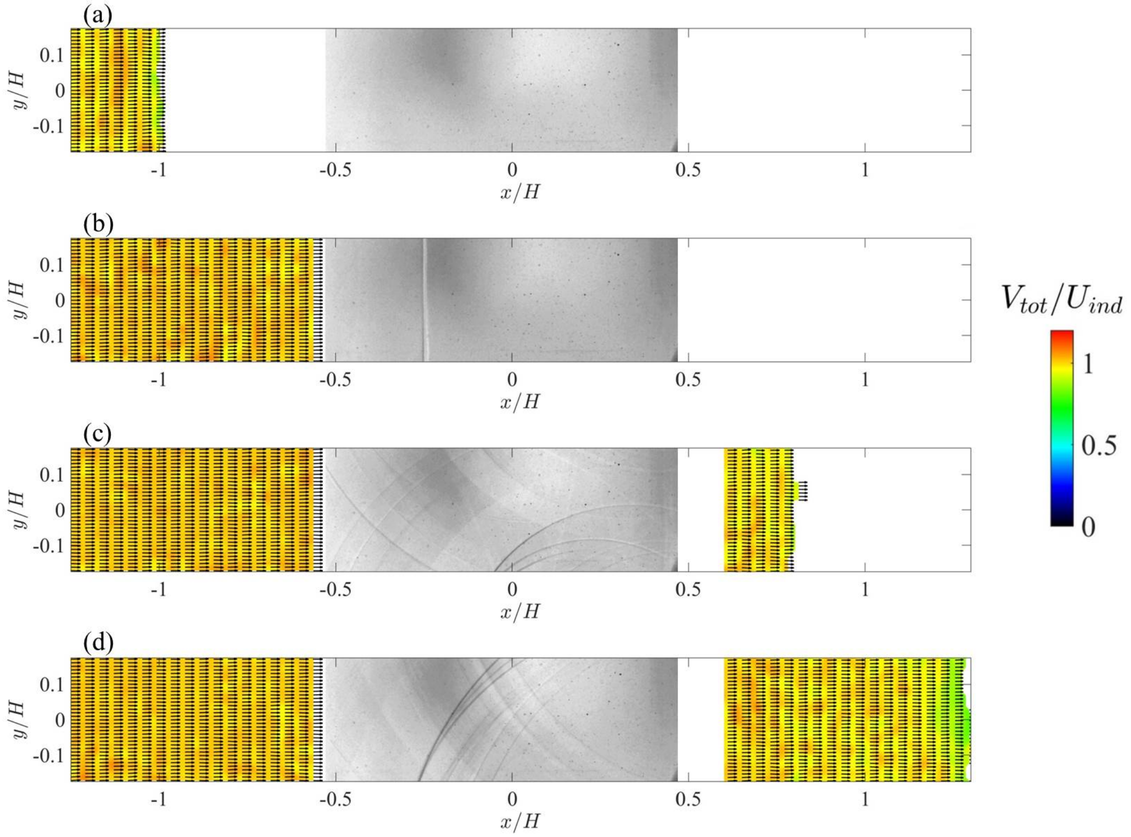

Figure 4. Core flow, without particle curtain, with shock wave a at $M_s = 1.40$, $t^* =$ (a) -0.43; (b) -0.10; (c) 0.30; (d) 0.50. Note that $x/H = 0$ corresponds to the center of the particle curtain slit.

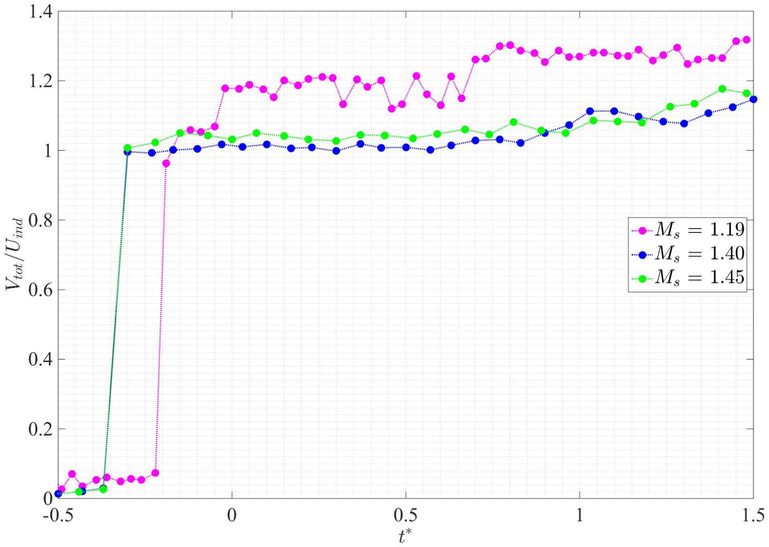

Figure 5. Increase in core flow as a function of time.

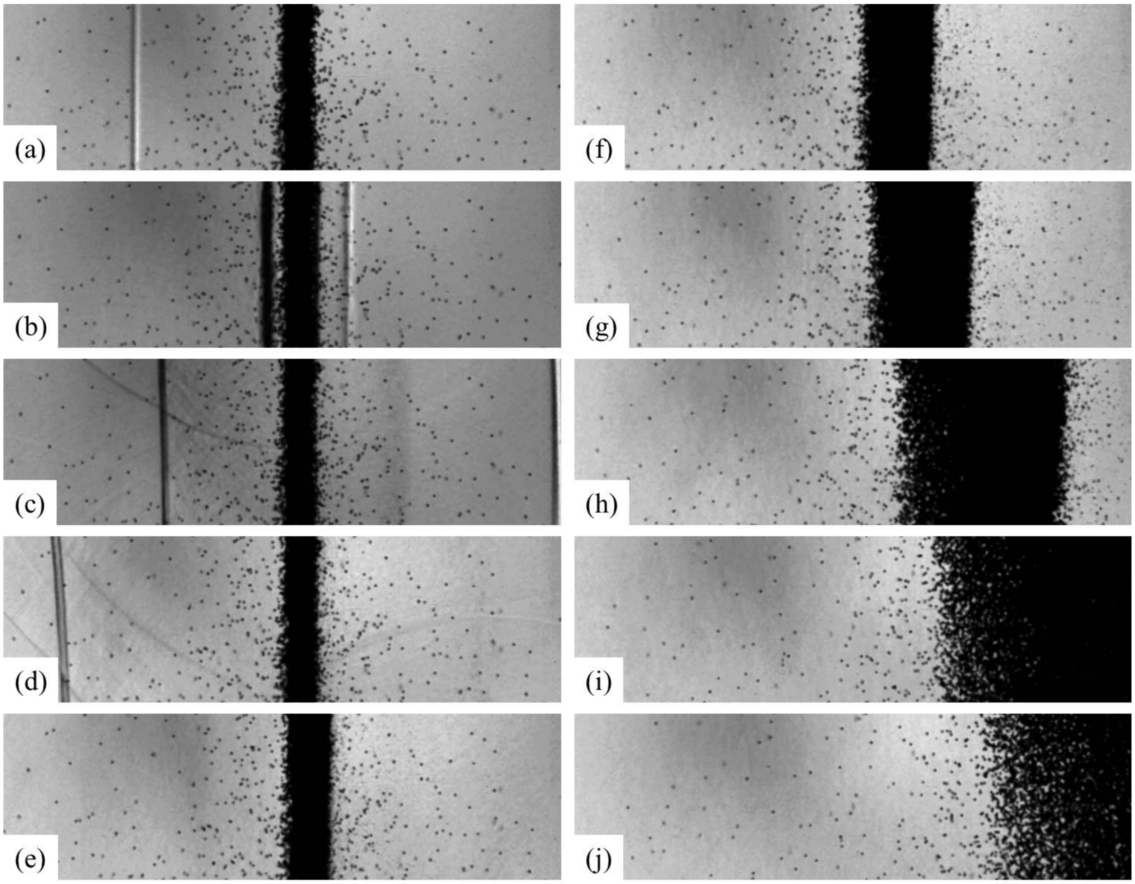

Figure 6. Schlieren imaging of the shock wave/particle curtain interaction: t^* = (a) -0.10; (b) 0.03; (c) 0.17; (d) 0.30 (curtain begins to deform); (e) 0.57; (f) 0.90; (g) 1.24; (h) 1.90; (i)2.57; (j) 3.24.

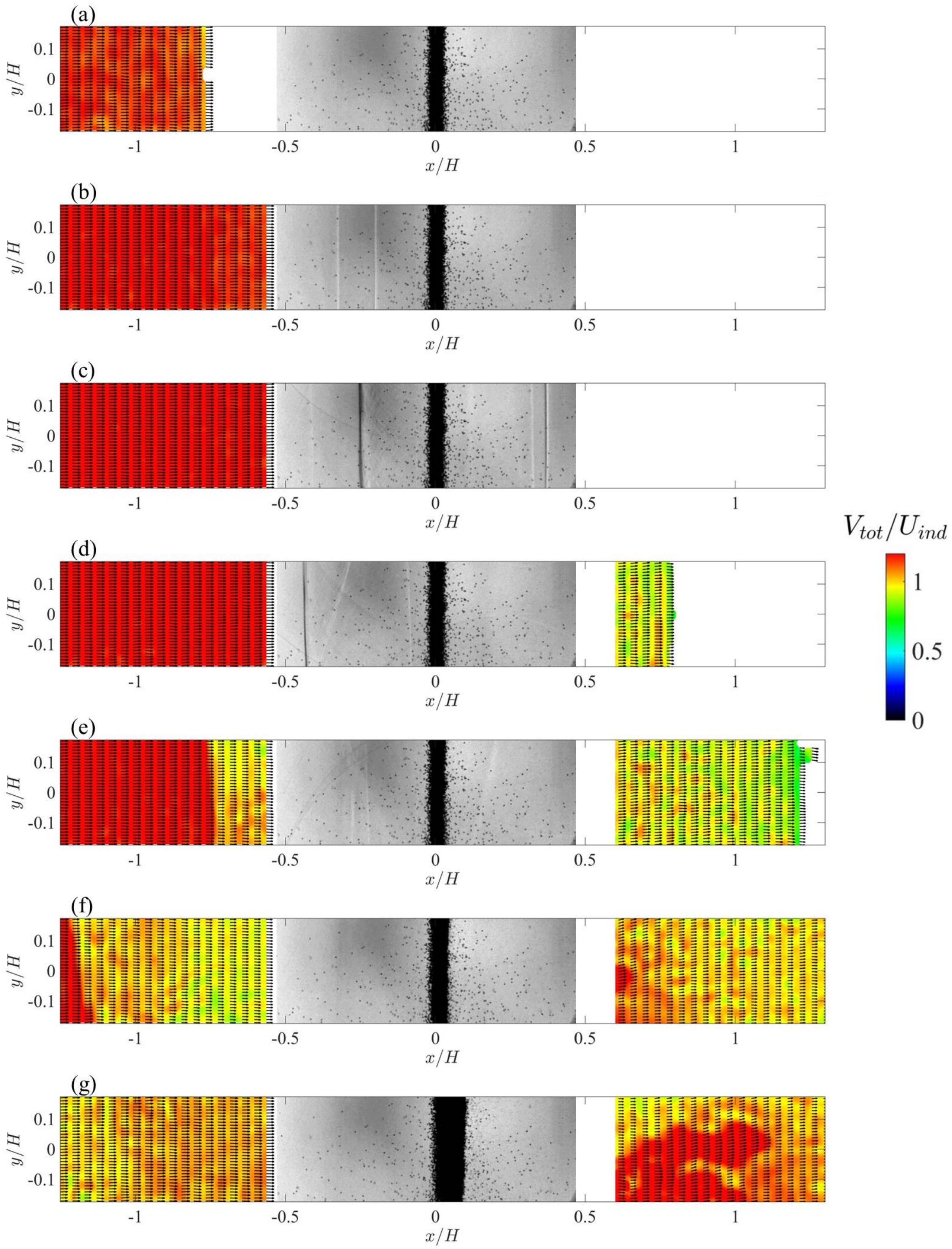

Figure 7. ***TR-PIV*** **color contours of total velocity with in-plane velocity vectors for $M_s = 1.19$ upstream and downstream of the particle curtain, with associated Schlieren at $t^* =$ (a) -0.22; (b) -0.05; (c) 0.09; (d) 0.15; (e) 0.26; (f) 0.43; (g) 0.80.**

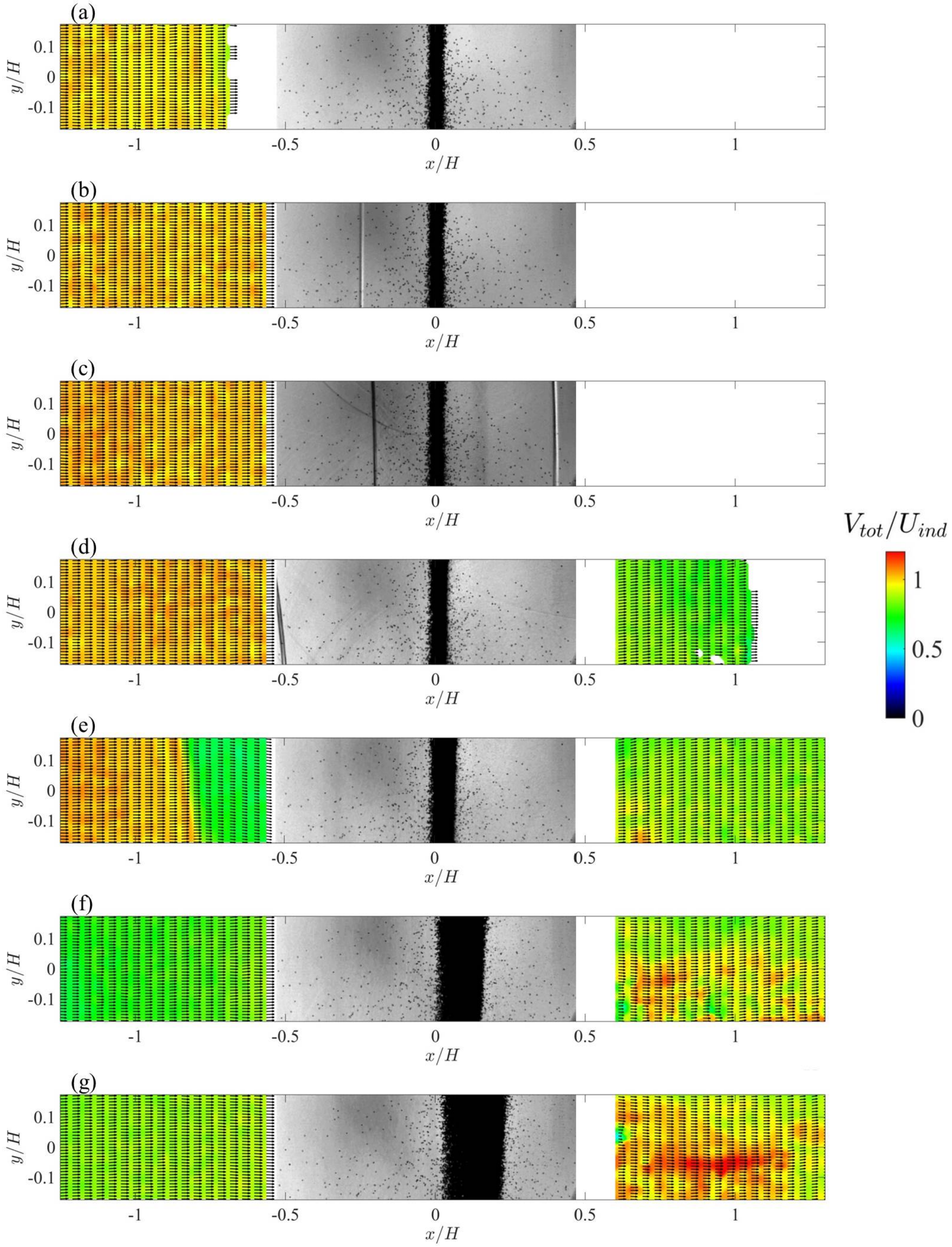

Figure 8. ***TR-PIV*** **color contours of total velocity with in-plane velocity vectors for $M_s = 1.40$ upstream and downstream of the particle curtain, with associated Schlieren at $t^* =$ (a) -0.30; (b) -0.10; (c) 0.17; (d) 0.43; (e) 0.70; (f) 1.24; (g) 1.57.**

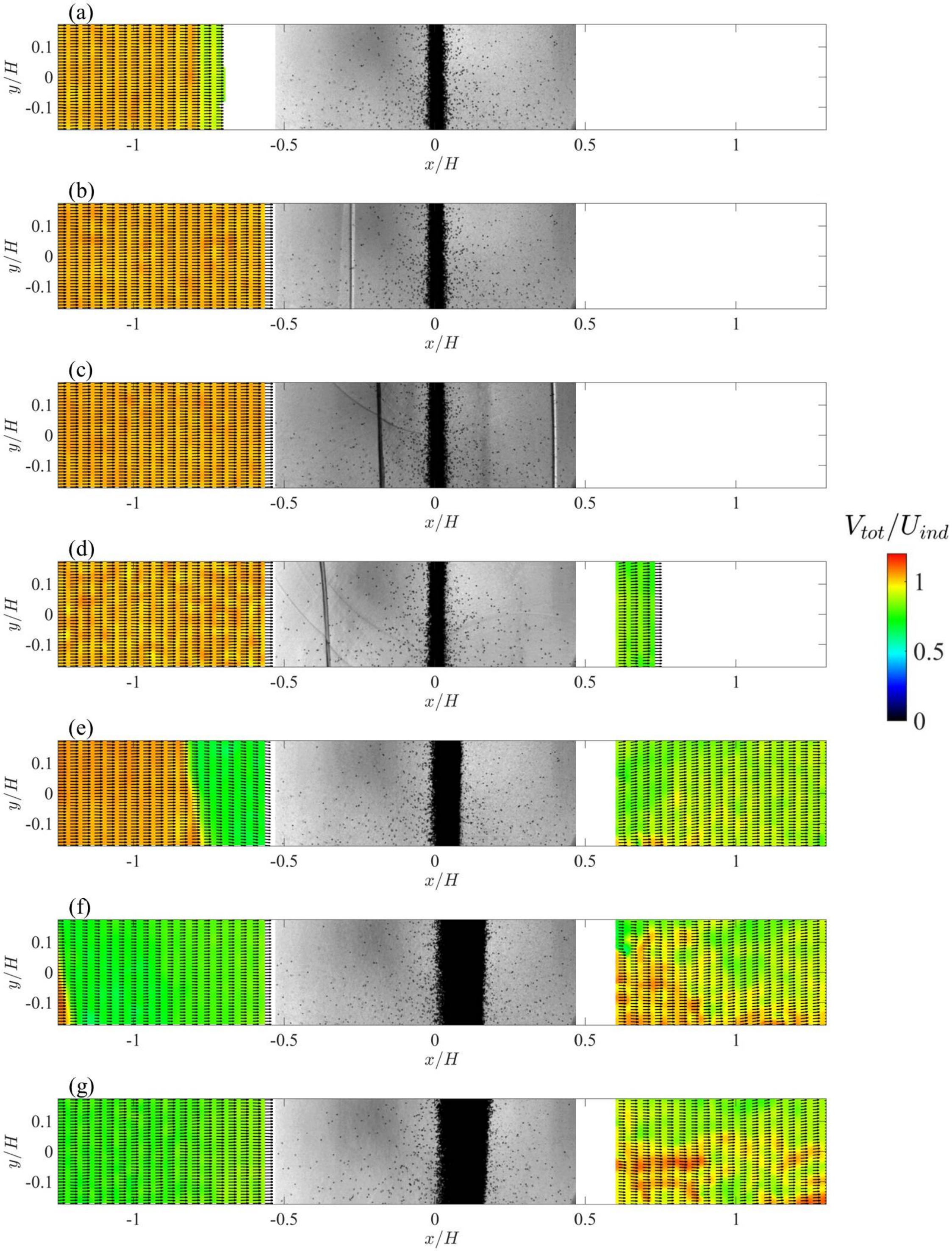

Figure 9. ***TR-PIV* color contours of total velocity with in-plane velocity vectors for $M_s = 1.45$ upstream and downstream of the particle curtain, with associated Schlieren at $t^* =$ (a) -0.30; (b) -0.07; (c) 0.22; (d) 0.44; (e) 0.81; (f) 1.26; (g) 1.55.**

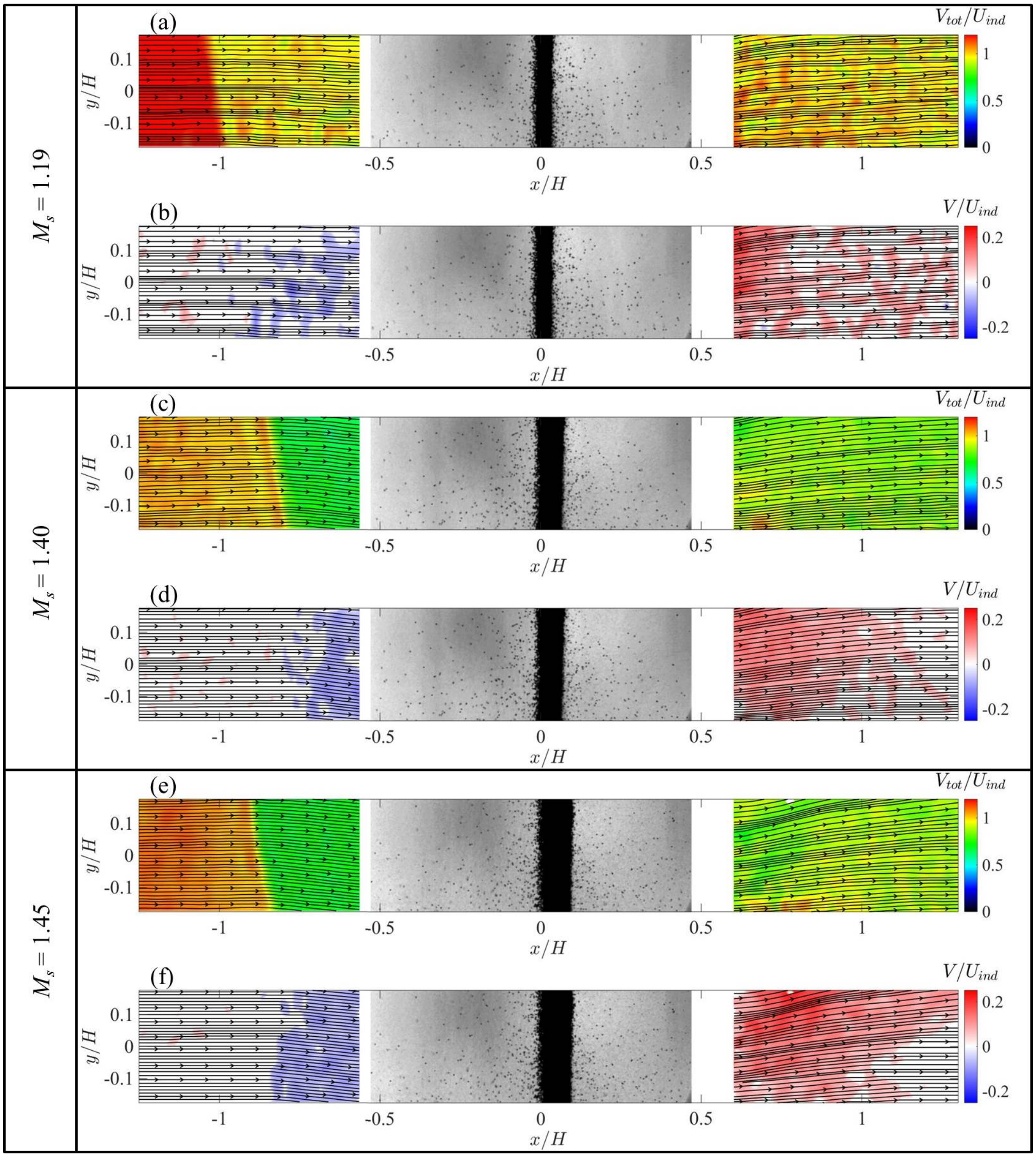

Figure 10. Color contours of V_{tot} with in-plane streamlines for M_s = (a) 1.19; (c) 1.40; (e) 1.45. Color contours of V-velocity with in-plane streamlines for M_s = (b) 1.19; (d) 1.40; (f) 1.45. These images correspond to t^* = (a, b) 0.36; (c, d) 0.70; (e, f) 0.89.

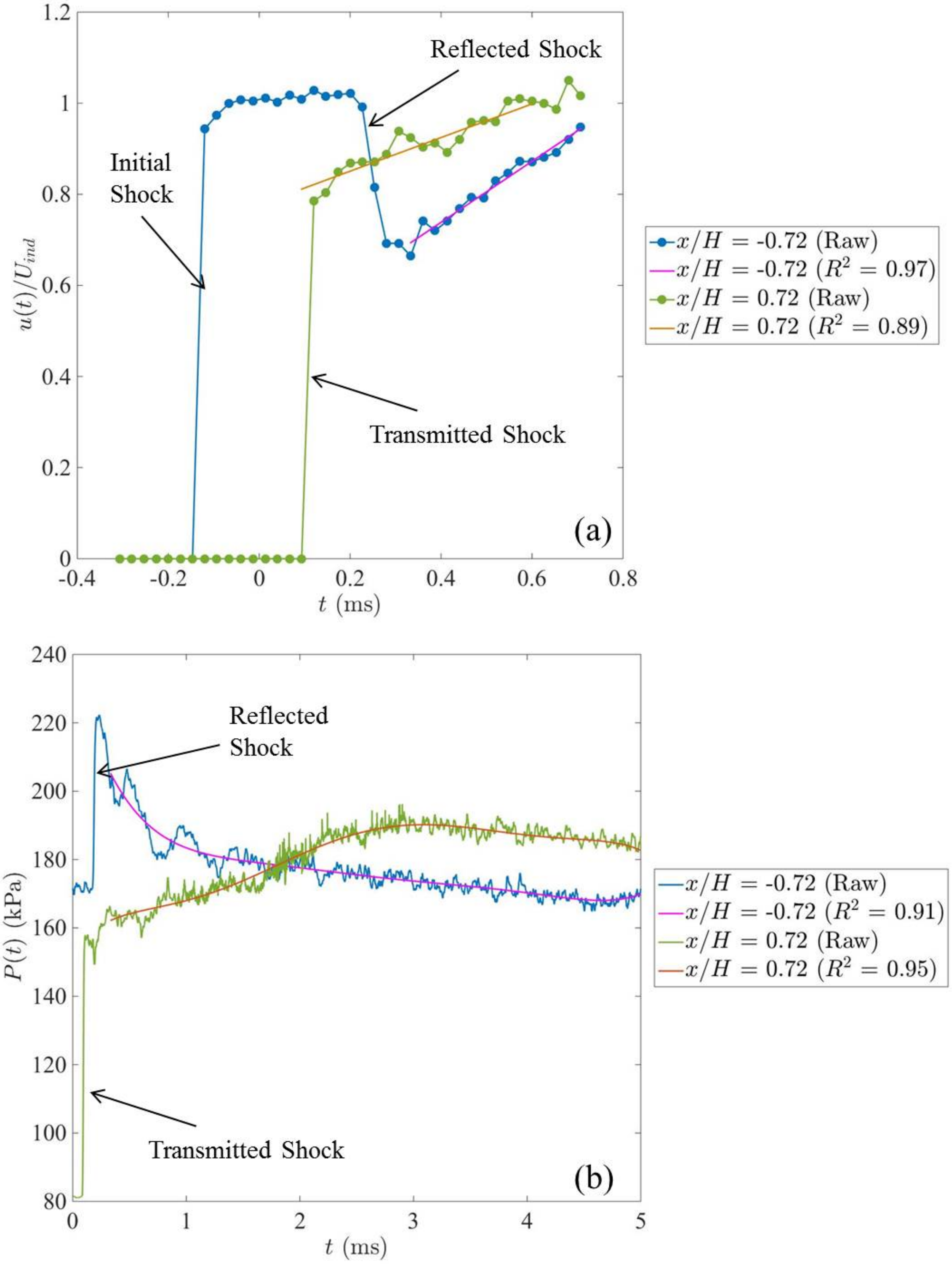

Figure 11. Time-traces and curve fits of the upstream and downstream (a) streamwise velocities (37.5 kHz) and (b) pressure taps (800 kHz), for $M_s = 1.40$. The time-traces represent the average of three runs. For drag calculations performed using Eq. (5), only data within the first 1 ms, after the passge of the reflected shock wave was utilized.

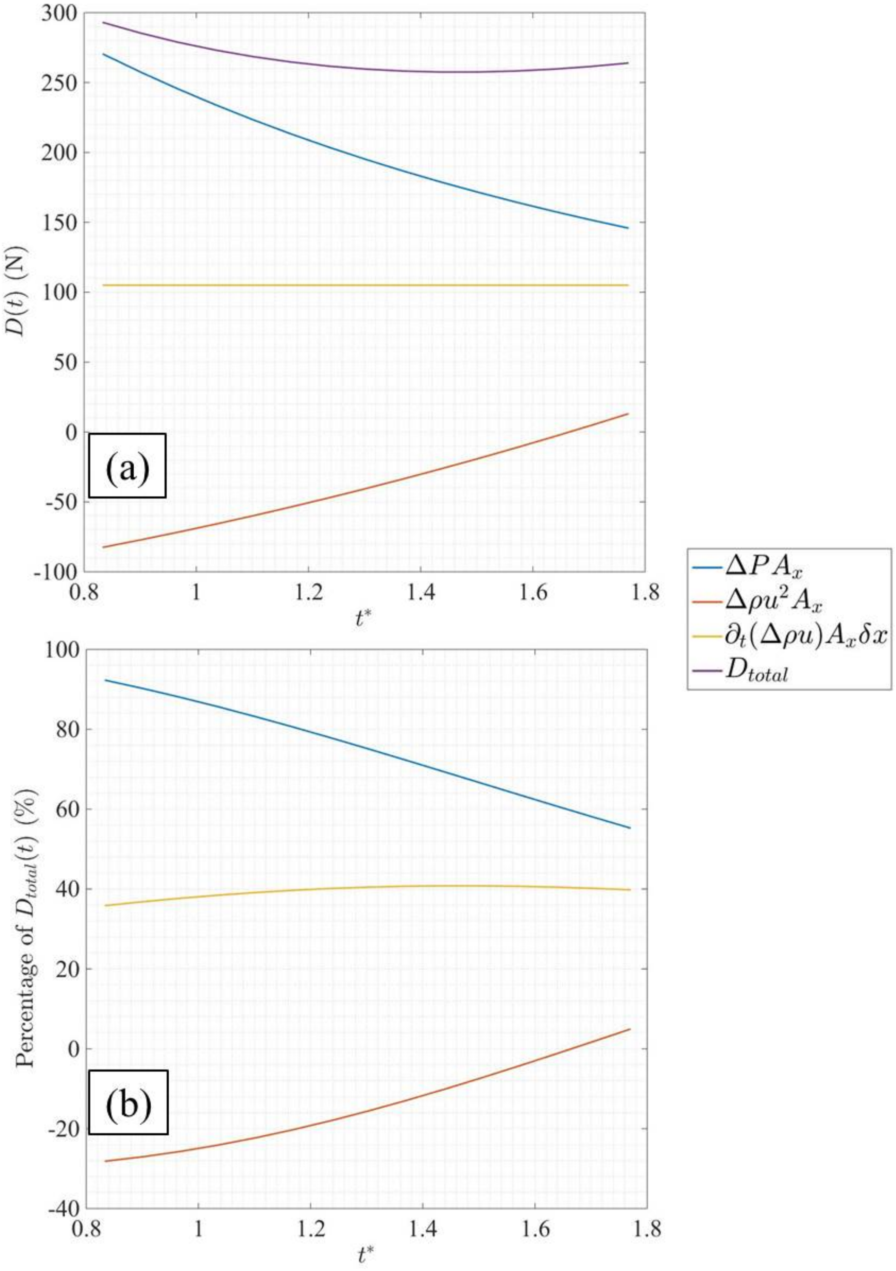

Figure 12. (a) Estimation for the change in drag as a function of time for the case where $M_s = 1.40$, along with the contributions of the different terms of Eq. (5); (b) percentage contribution to the total drag as a function of time.